Journal of Materials Science and Chemical Engineering, 2017, 5, 45-55
http://www.scirp.org/journal/msce
ISSN Online: 2327-6053
ISSN Print: 2327-6045

Enhancement of Oxygen Evolution Activity of Ruddlesden-Popper-Type Strontium Ferrite by Stabilizing Fe^{4+}

Toshihiro Takashima[1*], Koki Ishikawa[2], Hiroshi Irie[1]

[1]Clean Energy Research Center, University of Yamanashi, Yamanashi, Japan
[2]Special Doctoral Program for Green Energy Conversion Science and Technology, Interdisciplinary Graduate School of Medicine and Engineering, University of Yamanashi, Yamanashi, Japan
Email: *ttakashima@yamanashi.ac.jp

How to cite this paper: Takashima, T., Ishikawa, K. and Irie, H. (2017) Enhancement of Oxygen Evolution Activity of Ruddlesden-Popper-Type Strontium Ferrite by Stabilizing Fe^{4+}. *Journal of Materials Science and Chemical Engineering*, **5**, 45-55.
https://doi.org/10.4236/msce.2017.54005

Received: March 16, 2017
Accepted: April 27, 2017
Published: April 30, 2017

Abstract

Development of active iron based water oxidation for designing an ideal artificial photosynthesis devices operating under benign neutral pH is highly demanded. We investigated the electrocatalytic activity of Ruddlesden-Popper-type strontium ferrite ($Sr_3Fe_2O_7$) toward the oxygen evolution reaction (OER). Owing to the temperature-dependent efficiency of the charge disproportionation of Fe^{4+}, the OER activity of $Sr_3Fe_2O_7$ varied with the temperature, and the onset potential for the OER at a neutral pH underwent a negative shift of approximately 200 mV by increasing the temperature for the stabilization of Fe^{4+}. When metal substitution was made to $Sr_3Fe_2O_7$ for stabilizing Fe^{4+} at room temperature, the temperature dependence of the OER activity disappeared and the OER was driven at a small overpotential without increasing the temperature, indicating that the stabilization of Fe^{4+} is substantially important for achieving high OER activity.

Keywords

Oxygen Evolution, Charge Disproportionation, Water-Splitting, $Sr_3Fe_2O_7$

1. Introduction

The ever-growing global energy consumption has triggered considerable interest in addressing the challenge of storing renewable energy in a chemical form [1] [2]. One promising solution to this issue is to produce hydrogen (H_2) by using solar energy to split water into H_2 and oxygen (O_2) [3] [4] [5]. As a four-electron transfer reaction, the O_2 evolution reaction (OER, $2H_2O \rightarrow O_2 + 4H^+ + 4e^-$), which is a half-reaction of water splitting, suffers from sluggish kinetics

owing to a large overpotential and has been considered to be the efficiency-limiting step of water splitting. Therefore, extensive research has been devoted to developing O_2 evolution catalysts [6]-[15]. Iridium oxide (IrO_2) and ruthenium oxide (RuO_2) are effective OER catalysts for solar water splitting as they exhibit high turnover frequencies under neutral pH conditions [6] [7] [8]; however, their high cost and scarcity render their use impractical for large-scale applications. Thus, it is important to develop active OER catalysts using earth-abundant elements.

In the past few decades, many earth-abundant metal oxides have been investigated [9] [10] [11] as potential OER catalysts to replace IrO_2 and RuO_2. Among them, iron (Fe) oxide is attractive because Fe is the most abundant first-row transition metal on Earth and nontoxic. Several Fe-based OER catalysts have been reported to show excellent activity [12] [13] [14] [15]. For example, $Ba_{0.5}Sr_{0.5}Co_{0.8}Fe_{0.2}O_3\delta$ and $CaCu_3Fe_4O_{12}$ have high activity comparable to that of IrO_2 and RuO_2 in an alkaline solution [12] [13]. Despite these achievements; however, substantial improvements in the design and preparation of catalysts are still needed because few Fe-based OER catalysts function effectively under neutral pH conditions [16] [17] [18]. Therefore, for the successful application of Fe-based catalysts as components for solar fuel production systems, improvement of their OER activity under neutral pH conditions is essential.

Recently, numerous studies have been conducted to investigate the mechanism of the OER on Fe oxides by using various spectroelectrochemical techniques [18] [19] [20] [21] [22]. On the basis of the results of in situ UV-vis measurement, we have reported that Fe^{4+} is the intermediate species of the OER on a hematite (α-Fe_2O_3) electrode [18] [19]. Hamann *et al.* observed a potential- dependent infrared absorption peak, which they attributed to a high-valent Fe^{4+}-oxo species, and proposed that the rate-determining step of the OER is Fe^{3+}-OH → $Fe^{4+} = O + e^- + H^+$ [20]. Chen *et al.* conducted in situ Mössbauer measurements and observed signals indicating that the formation of Fe^{4+} proceeds on NiFe hydroxide during the electrocatalysis of the OER [21]. Concerning a descriptor for OER activity, Suntivich et al. reported that near-unity occupancy of the eg orbitals of transition-metal ions at the B-site of perovskites (formula ABO_3) is essential to obtain high OER activity [12]. Notably, the Fe^{4+} ion that is formed on metal oxides has the high-spin d^4 configuration of $t_{2g}^3e_g^1$ [23] [24], and its formation satisfies the conditions required for high OER activity. On the basis of these reports, we hypothesize that the accessibility to Fe^{4+} is a possible descriptor for the OER activity of Fe-based catalysts [25]. Ruddlesden-Popper-type strontium ferrite ($Sr_3Fe_2O_7$) contains Fe^{4+} which is unstable and consumed by charge disproportionation (CD) ($2Fe^{4+} \rightarrow Fe^{3+} + Fe^{5+}$) [26]. Notably, the CD of Fe^{4+} in $Sr_3Fe_2O_7$ can be suppressed by regulating the temperature and its chemical composition [26] [27] [28].

Thus, to examine the validity of the hypothesis that the accessibility to Fe^{4+} is a descriptor for the OER activity of Fe-based catalysts, we have investigated the OER activities of $Sr_3Fe_2O_7$ and its La- or Ti-substituted compounds at different

temperatures using electrochemical measurements. By increasing the temperature or substituting the foreign elements to suppress the CD of Fe^{4+}, the enhancement of the OER activity was observed.

2. Experimental Section

2.1. Preparation of Electrodes

$Sr_3Fe_2O_7$ powder was synthesized by a solid-state reaction [26]. Stoichiometric amounts of α-Fe_2O_3 (Kojundo Chemical Lab., 99.9%) and strontium carbonate ($SrCO_3$, Kojundo Chemical Lab., 99.9%) were ground in a ball mill and calcinated in air at 900˚C for 9 h. The resulting powder was pressed into pellets and sintered in air at 1300˚C for 24 h. When $Sr_{2.6}La_{0.4}Fe_2O_7$ and Sr_3FeTiO_7 were prepared, stoichiometric amounts of lanthanum oxide (La_2O_3, Kanto Chemical, 98.0%) and titanium dioxide (TiO_2, Kanto Chemical, 98.0%) were added to the starting materials as reported in the literature [27] [28]. All chemical reagents were used without further purification.

Electrodes were prepared using a spray deposition method as reported previously [25]. Briefly, 300 mg of the synthesized powder sample was suspended in 200 mL of ethanol. The suspension was sprayed onto a clean conducting glass substrate (FTO-coated glass, resistance: 20 Ω/square; SPD Laboratory Inc.) at 170˚C using an automatic spray gun (Lumina, ST-6; Fuso Seiki Co., Ltd.). After coating, the resultant transparent black film was calcinated at 500 ºC in air for 2 h.

2.2. Characterization

The crystal structures of the electrocatalysts were analyzed by X-ray diffraction (XRD) using a PW-1700 X-ray diffractometer (PANalytical) with monochromatic Cu Kα radiation. XRD patterns were recorded from 15˚ to 80˚ in 2θ with a step size of 0.02˚ and a scan rate of 0.25˚/min. Scanning electron microscopy (SEM) inspection was performed using a scanning electron microscope (JSM-6500F, JEOL).

2.3. Electrochemical Measurements

Polarization curves were obtained with a commercial potentiost at and potential programmer (HZ-5000, Hokuto Denko). A platinum wire was used as a counter electrode. All potentials were measured against a silver/silver chloride reference electrode (Ag/AgCl/KCl(sat.)) and converted to the standard hydrogen electrode (SHE) reference scale using the equation U(versus SHE) = U(versus Ag/AgCl/KCl (sat.)) + 0.197. The electrolyte solution used for all experiments was 0.1 M sodium sulfate (Na_2SO_4) aqueous solution, which was prepared from highly pure Milli-Q water (18 MΩ·cm) and Na_2SO_4 (Kanto Kagaku, 99.0%). The pH was adjusted to 7 using 0.1 M sulfuric acid (H_2SO_4, Kanto Kagaku, 96.0%) and 0.1 M sodium hydroxide (NaOH, Kanto Kagaku, 97.0%). No agent for pH buffering was added to the electrolyte solution to avoid effects from the adsorption of multivalent anions. Prior to the measurement, the electrolyte was maintained at

a certain temperature and bubbled with argon gas for at least 15 min. Polarization curves were measured by sweeping the electrode potential from the rest potential to 1.5 V at a scan rate of 10 mV/s and the concentration of O_2 dissolved in the electrolyte was monitored during the potential sweep using a needle-type O_2 microsensor (Microx TX3-trace, PreSens). The current density was normalized to the geometric surface area of the electrode.

3. Results and Discussion

3.1. Characterization of the Prepared Electrodes

Figure 1 shows the XRD patterns of $Sr_3Fe_2O_7$ and its substituted materials $Sr_{2.6}La_{0.4}Fe_2O_7$ and Sr_3FeTiO_7. All materials exhibited XRD patterns indexed to the tetragonal space group I4/mmm as reported in the literature [26] [27] [28], and no peaks assignable to other crystal phases were detected. The peak position of the prepared $Sr_3Fe_2O_7$ (Figure 1(a)) matched with a reference data (Figure 1(b), ICSD no. 163173). In contrast, the intensity of the diffraction peaks corresponding to (00*h*) planes was particularly intense for our prepared $Sr_3Fe_2O_7$. This can be understood by the preferred orientation of the $Sr_3Fe_2O_7$ particles which have plate-like shapes (Figure 2(a)) owing to its two-dimensional (2-D)

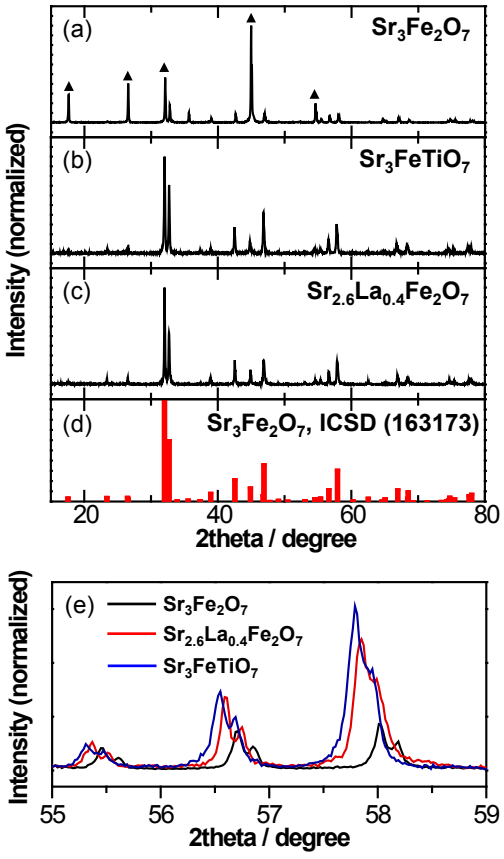

Figure 1. XRD patterns of synthesized crystalline powder ((a) $Sr_3Fe_2O_7$; (b) $Sr_{2.6}La_{0.4}Fe_2O_7$ and (c) Sr_3FeTiO_7) and (d) reference data ($Sr_3Fe_2O_7$, ICSD no. 163173). Peaks marked with (▲) in trace (a) correspond to (00*h*) diffraction peaks. (e) Shift of diffraction peaks to a lower angle upon substituting metal ions.

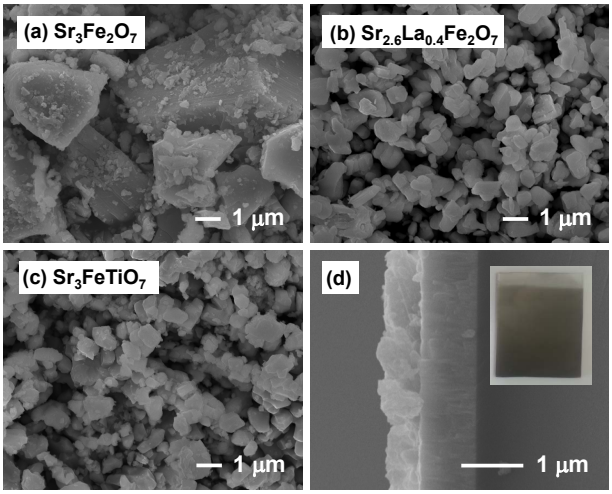

Figure 2. SEM images of the prepared electrodes ((a) $Sr_3Fe_2O_7$; (b) $Sr_{2.6}La_{0.4}Fe_2O_7$ and (c) Sr_3FeTiO_7); (d) Cross-section image of a $Sr_3Fe_2O_7$ electrode. The inset of (d) shows an optical image of the $Sr_3Fe_2O_7$ electrode.

layered crystal structure composed of stacked rock salt and perovskite layers with the sequence of SrO-$(SrFeO_3)_2$. For $Sr_{2.6}La_{0.4}Fe_2O_7$ and Sr_3FeTiO_7, shifts of the diffraction peaks to lower angles were observed (**Figure 1(e)**), confirming that cationic substitution had taken place. The peak shift was larger for Sr_3FeTiO_7 as the expansion of the crystal lattice has been reported to be more prominent for Sr_3FeTiO_7 than $Sr_{2.6}La_{0.4}Fe_2O_7$ [27] [28].

Figure 2 shows SEM images of the prepared film electrodes. The $Sr_3Fe_2O_7$ particles had a diameter ranging from 1 μm to 8 μm (**Figure 2(a)**). In contrast, the particle sizes of $Sr_{2.6}La_{0.4}Fe_2O_7$ and Sr_3FeTiO_7 were approximately from 0.3 μm to 1.2 μm (**Figure 2(b)** and **Figure 2(c)**). All the samples were uniformly deposited on the electrodes. From the cross-section image in **Figure 2(d)**, the thickness of the deposited film was found to be approximately 500 nm.

3.2. Electrocatalytic Activity of $Sr_3Fe_2O_7$ Electrocatalysts

Figure 3 shows polarization curves of a $Sr_3Fe_2O_7$ film electrode measured at pH 7. Irrespective of the temperature, we observed simultaneous increases in the anodic current and O_2 concentration while neither of them was observed at this potential by using a bare FTO electrode (data not shown). In contrast to the typical polarization curves for OER, $Sr_3Fe_2O_7$ showed a slight decrease in the anodic current upon sweeping the electrode potential. This decrease is because a part of $Sr_3Fe_2O_7$ transformed to $Sr_3Fe_2(OH)_{12}$ during the measurements by intercalation of water molecules between its two rock-salt-type SrO layers [29]. However, because this transformation causes no anodic current and O_2 formation, we can consider that the observed results indicate that the OER was electrocatalyzed on $Sr_3Fe_2O_7$.

Notably, when the temperature of the electrolyte was increased from 30˚C to 70˚C, the anodic current showed a negative shift of the onset potential of approximately 200 mV. Since the onset potential for O_2 formation was similarly

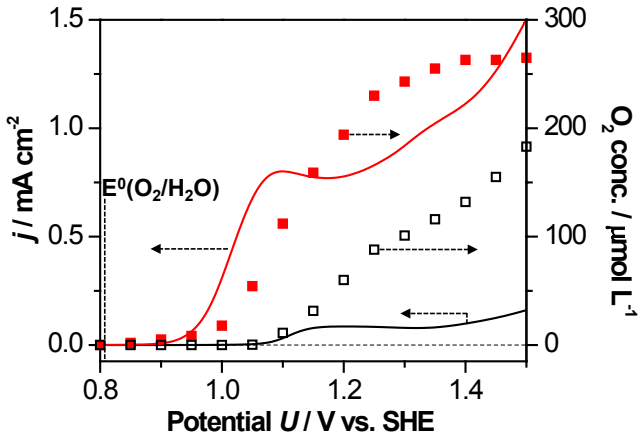

Figure 3. Potential dependences of current density (line) and dissolved O_2 concentration (squares) for $Sr_3Fe_2O_7$ electrodes in 0.1 M Na_2SO_4 aqueous solution (pH 7) during a potential sweep at 10 mV/s at 70˚C (red line and closed squares) and 30˚C (black line and open squares). E˚ represents the standard potential of the OER at pH 7.

shifted, these results indicate that the OER activity of $Sr_3Fe_2O_7$ is improved by increasing the temperature. As demonstrated in a solid oxide electrolysis cell (SOEC), the OER is thermodynamically more favorable at a high temperature and the standard potential of the OER becomes more negative with increasing temperature owing to a decrease in the Gibbs free energy required for the OER [30]. However, the potential shift due to the change in the Gibbs free energy is estimated to be at most only 40 mV at 70˚C because of the small temperature difference between 30˚C and 70˚C. Thus, the observed improvement of the OER activity should originate from a temperature-dependent property of $Sr_3Fe_2O_7$.

As described in the introduction, Fe^{4+} is considered to play an important role in the OER on Fe-based catalysts; however, Fe^{4+} is unstable against CD and rapidly disappears in usual [26] [28] [29] [31] [32] [33] According to the literature, the efficiency of CD is closely related to the electronic bandwidth of σ* bonding composed of Fe-3d and O-2pσ* orbitals, and CD occurs when the bandwidth of σ* bonding is narrow [31] [32]. For Fe-based perovskite compounds, the bandwidth broadens at high temperatures because with increasing temperature, the Fe-O-Fe bond angle increases and the electronic interaction between Fe and O strengthens [31] [32]. Kuzushita *et al.* investigated the temperature dependence of the Fe^{4+} stability by performing Mössbauer measurements and found that there is a critical temperature for the CD of $Sr_3Fe_2O_7$ at 70˚C ± 10˚C, indicating that CD is suppressed above 70˚C [26]. Therefore, the observed enhancement of OER activity at 70˚C is considered to be due to the suppression of the CD of Fe^{4+}.

To examine the validity of the interpretation that the stabilization of Fe^{4+} leads to the enhancement of the OER activity of $Sr_3Fe_2O_7$, we also investigated the effect of Fe^{4+} stability on the OER activity using the metal-substituted materials. **Figure 4(a)** shows the polarization curves of $Sr_{2.6}La_{0.4}Fe_2O_7$ measured at 30˚C and 70˚C. Unlike $Sr_3Fe_2O_7$, the anodic current initiated to increase from essentially the same potential for both temperatures, which is consistent with the

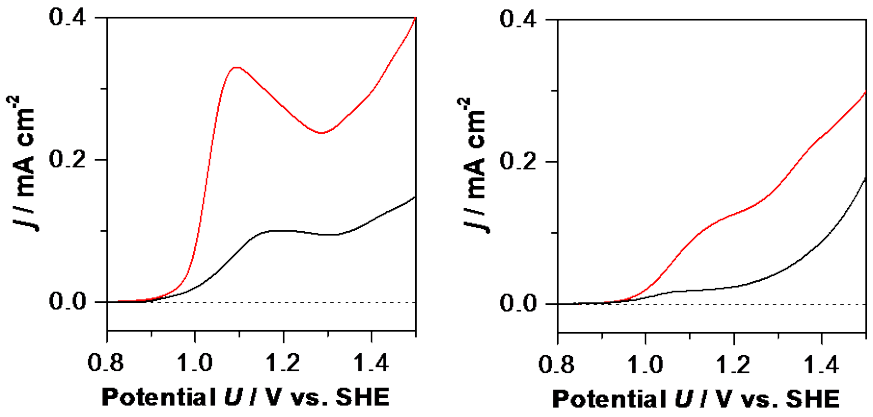

(a) (b)

Figure 4. Polarization curves of (a) $Sr_{2.6}La_{0.4}Fe_2O_7$ and (b) Sr_3FeTiO_7 electrodes measured at 70˚C (red line) and 30˚C (black line).

fact that the substitution of Sr with La suppresses CD at room temperature and that Fe^{4+} in $Sr_{2.6}La_{0.4}Fe_2O_7$ is stable at both 30˚C and 70˚C [27]. When the OER was conducted with Sr_3FeTiO_7, in which Fe^{4+} is stably contained at room temperature [28], the onset potential was independent of temperature. Thus, the stabilization of Fe^{4+} is an effective means of enhancing the OER activity of Fe oxide. As shown in **Figure 4(a)** and **Figure 4(b)**, a higher current density was observed at 70˚C.

Although the reason for this is unclear, it is assumed to be due to the greater convection of the electrolyte. Notably, the onset potentials observed with these substituted materials were almost the same as that observed for $Sr_3Fe_2O_7$ at 70˚C, indicating that the efficient formation of Fe^{4+} on $Sr_3Fe_2O_7$ derivatives enables the initiation of the OER around this potential. From a comparison of the polarization curves (**Figure 3**, **Figure 4(a)** and **Figure 4(b)**), the current density of $Sr_3Fe_2O_7$ at 70˚C was larger than those of metal substituted derivatives at the same temperature. This is likely to be due to higher concentration of Fe^{4+} in $Sr_3Fe_2O_7$.

From the above results, the OER activity of $Sr_3Fe_2O_7$ derivatives is considered to be determined by the efficiency of Fe^{4+} formation, and the suppression of CD was found to be effective for designing active OER catalysts. CD is known to take place not only with Fe^{4+} but also with other first-row transition-metal ions [31] [32]. Previously, one of the authors (T. T.) showed that the CD of Mn^{3+} is the primary origin of the pH-dependent OER activity of MnO_2 and succeeded in enhancing OER activity under a neutral pH by suppressing CD [34] [35] [36]. Thus, by analogy with Fe^{4+} and Mn^{3+}, the stabilization of other first-row transition-metal ions by suppressing CD is likely to be a promising approach for the development of active OER catalysts made from abundant elements. Fe ions introduced in layer-structured metal (hydr) oxides have been reported to form Fe^{4+} without causing CD [37] [38]. The application of Fe-doped layered materials to the OER is currently underway in our laboratory.

4. Conclusion

In this study, the OER activity of $Sr_3Fe_2O_7$ was investigated at 30˚C and 70˚C under neutral pH conditions. The onset potential for the OER of a $Sr_3Fe_2O_7$ electrode was found to be dependent on the temperature and shifted by approximately 200 mV in the negative direction with increasing temperature. This enhancement of the OER activity is considered to be due to the fact that Fe^{4+} is stably formed by suppressing CD at 70˚C, and the stabilization of Fe^{4+} by metal substitution enabled efficient OER catalysis at room temperature. Unfortunately, $Sr_3Fe_2O_7$ derivatives underwent the transformation in aqueous solution; however, these findings will provide insights for designing Fe oxide OER catalysts that can evolve O_2 efficiently under neutral pH conditions.

Acknowledgements

This work was financially supported by the Program to Disseminate Tenure Tracking System by MEXT and by JKA with promotion funds from KEIRIN RACE (28-146).

References

[1] Gray, H.B. (2009) Powering the Planet with Solar Fuel. *Nature Chemistry*, **1**, 7. https://doi.org/10.1038/nchem.141

[2] Lewis, N.S. and Nocera, D.G. (2006) Powering the Planet: Chemical Challenges in Solar Energy Utilization. *Proceedings of the National Academy of Sciences*, **103**, 15729-15735. https://doi.org/10.1073/pnas.0603395103

[3] Fujishima, A. and Honda, K. (1972) Electrochemical Photolysis of Water at a Semiconductor Electrode. *Nature*, **238**, 37-38. https://doi.org/10.1038/238037a0

[4] Meyer, T. (2008) Catalysis: The Art of Splitting Water. *Nature*, **451**, 778. https://doi.org/10.1038/451778a

[5] Walter, M.G., Warren, E.L., McKone, J.R., Boettcher, S.W., Mi, Q., Santori, E.A. and Lewis, N.S. (2010) Solar Water Splitting Cells. *Chemical Reviews*, **110**, 6446-6473. https://doi.org/10.1038/451778a

[6] Lee, Y., Suntivich, J., May, K.J., Perry, E.E. and Shao-Horn, Y. (2012) Synthesis and Activities of Rutile IrO_2 and RuO_2 Nanoparticles for Oxygen Evolution in Acid and Alkaline Solutions. *The Journal of Physical Chemistry Letters*, **3**, 399-404. https://doi.org/10.1021/jz2016507

[7] Chao, Y., Hernandez-Pagan, E.A., Vargas-Barbosa, N.M., Dysart, J.L. and Mallouk, T.E. (2011) A High Yield Synthesis of Ligand-Free Iridium Oxide Nanoparticles with High Electrocatalytic Activity. *The Journal of Physical Chemistry Letters*, **2**, 402-406. https://doi.org/10.1021/jz200051c

[8] Chandra, D., Takama, D., Masaki, T., Sato, T., Abe, T., Togashi, T., Kurihara, M., Saito, K., Yui, T. and Yagi, M. (2016) Highly Efficient Electrocatalysis and Mechanistic Investigation of Intermediate $IrO_x(OH)_y$ Nanoparticle Films for Water Oxidation. *ACS Catalysis*, **6**, 3946-3954. https://doi.org/10.1021/acscatal.6b00621

[9] Jin, K., Chu, A., Park, J., Jeong, D., Jerng, S.E., Sim, U., Jeong, H.-Y., Lee, C.W., Park, Y.-S., Yang, K.D., Pradhan, G.K., Kim, D., Sung, N.-E., Kim, S.H. and Nam, K.T. (2015) Partially Oxidized Sub-10 nm MnO Nanocrystals with High Activity for Water Oxidation Catalysis. *Scientific Reports*, **5**, 10279.

https://doi.org/10.1038/srep10279

[10] McCrory, C.C.L., Jung, S., Peters, J.C. and Jaramillo, T.F. (2013) Benchmarking Heterogeneous Electrocatalysts for the Oxygen Evolution Reaction. *Journal of the American Chemical Society*, **135**, 16977-16987. https://doi.org/10.1021/ja407115p

[11] Hunter, B.M., Gray, H.B. and Müller, A.M. (2016) Earth-Abundant Heterogeneous Water Oxidation Catalysts. *Chemical Reviews*, **116**, 14120-14136. https://doi.org/10.1021/acs.chemrev.6b00398

[12] Suntivich, J., May, K.J., Gasteiger, H.A., Goodenough, J.B. and Shao-Horn, Y. (2011) A Perovskite Oxide Optimized for Oxygen Evolution Catalysis from Molecular Orbital Principles. *Science*, **334**, 1383-1385. https://doi.org/10.1126/science.1212858

[13] Yagi, S., Yamada, I., Tsukasaki, H., Seno, A., Murakami, M., Fujii, H., Chen, H., Umezawa, N., Abe, H., Nishiyama, N. and Mori, S. (2015) Covalency-Reinforced Oxygen Evolution Reaction Catalyst. *Nature Communications*, **6**, 8249. https://doi.org/10.1038/ncomms9249

[14] Smith, R.D.L., Prévot, M.S., Fagan, R.D., Zhang, Z., Sedach, P.A., Siu, M.K.J., Trudel, S. and Berlinguette, C.P. (2013) Photochemical Route for Accessing Amorphous Metal Oxide Materials for Water Oxidation Catalysis. *Science*, **340**, 60-63. https://doi.org/10.1126/science.1233638

[15] Townsend, T.K., Sabio, E.M., Browning, N.D. and Osterloh, F.E. (2011) Photocatalytic Water Oxidation with Suspended Alpha-Fe_2O_3 Particles-Effects of Nanoscaling. *Energy & Environmental Science*, **4**, 4270-4275. https://doi.org/10.1039/c1ee02110a

[16] Görlin, M., Gliech, M., De Araújo, J.F., Dresp, S., Bergmann, A. and Strasser, P. (2016) Dynamical Changes of a Ni-Fe Oxide Water Splitting Catalyst Investigated at Different pH. *Catalysis Today*, **262**, 65-73.

[17] Trześniewski, B.J., Diaz-Morales, O., Vermass, D.A., Longo, A., Bras, W., Koper, M.T.M. and Smith, W.A. (2015) *In Situ* Observation of Active Oxygen Species in Fe-Containing Ni-Based Oxygen Evolution Catalysts: The Effect of pH on Electrochemical Activity. *Journal of the American Chemical Society*, **137**, 15112-15121. https://doi.org/10.1039/c1ee02110a

[18] Takashima, T., Ishikawa, K. and Irie, H. (2016) Detection of Intermediate Species in Oxygen Evolution on Hematite Electrodes Using Spectroelectrochemical Measurements. *The Journal of Physical Chemistry C*, **120**, 24827-24834. https://doi.org/10.1021/acs.jpcc.6b07978

[19] Takashima, T., Ishikawa, K. and Irie, H. (2016) Efficient Oxygen Evolution on Hematite at Neutral pH Enabled by Proton-Coupled Electron Transfer. *Chemical Communications*, **52**, 14015-14018. https://doi.org/10.1039/C6CC08379J

[20] Zandi, O. and Hamann, T.W. (2016) Determination of Photoelectrochemical Water Oxidation Intermediates on Haematite Electrode Surfaces Using Operando Infrared Spectroscopy. *Nature Chemistry*, **8**, 778-783. https://doi.org/10.1038/nchem.2557

[21] Chen, J.Y., Dang, L., Liang, H., Bi, W., Gerken, J.B., Jin, S., Alp, E.E. and Stahl, S.S. (2015) Operando Analysis of NiFe and Fe Oxyhydroxide Electrocatalysts for Water Oxidation: Detection of Fe^{4+} by Mössbauer Spectroscopy. *Journal of the American Chemical Society*, **137**, 15090-15093. https://doi.org/10.1038/nchem.2557

[22] Barroso, M., Mesa, C.A., Pendlebury, S.R., Cowan, A.J., Hisatomi, T., Sivula, K., Grätzel, M., Klug, D.R. and Durrant, J.R. (2012) Dynamics of Photogenerated Holes in Surface Modified-Fe_2O_3 Photoanodesfor Solar Water Splitting. *Proceedings of the National Academy of Sciences*, **109**, 15640-15645. https://doi.org/10.1073/pnas.1118326109

[23] Bocquet, A.E., Suga, S., Kimizuka, N., Takeda, Y. and Takano, M. (1992) Electronic Structure of $SrFe^{4+}O$ and Related Fe Perovskite Oxides. *Physical Review B*, **45**, 1561-1570. https://doi.org/10.1103/PhysRevB.45.1561

[24] Yabuuchi, N. and Komaba, S. (2014) Recent Research Progress on Iron- and Manganese-Based Positive Electrode Materials for Rechargeable Sodium Batteries. *Science and Technology of Advanced Materials*, **15**, Article ID: 043501. https://doi.org/10.1088/1468-6996/15/4/043501

[25] Takashima, T., Ishikawa, K. and Irie, H. (2014) Thermal Activiation of $Sr_3Fe_2O_7$ Electrocatalysts for Water Oxidation at Neutral pH. *ECS Transactions*, **61**, 35-41. https://doi.org/10.1088/1468-6996/15/4/043501

[26] Kuzushita, K., Morimoto, S., Nasu, S. and Nakamura, S. (2000) Charge Disproportionation and Antiferromagnetic Order of $Sr_3Fe_2O_7$. *Journal of the Physical Society of Japan*, **69**, 2767-2770. https://doi.org/10.1143/JPSJ.69.2767

[27] Adler, P. (1997) Electronic State, Magnetism, and Electrical Transport Behavior of $Sr_{3-x}A_xFe_2O_7$ ($x \leq 0.4$, A = Ba, La). *Journal of Solid State Chemistry*, **130**, 129-139. https://doi.org/10.1006/jssc.1997.7289

[28] Adler, P. (1999) Charge Disproportionation in Iron (IV) Oxides: Electronic Properties and Magnetism in $Sr_3Fe_{2-x}Ti_xO_{7-y}$ Annealed at High Oxygen Pressures. *Journal of Materials Chemistry*, **9**, 471-477. https://doi.org/10.1039/a806772d

[29] Matvejeff, M., Lehtimäki, M., Hirasa, A., Huang, Y.-H., Yamauchi, H. and Karppinen, M. (2005) New Water-Containing Phase Derived from the$Sr_3Fe_2O_{7-}$ Phase of the Ruddlesden-Popper Structure. *Chemistry of Materials*, **17**, 2775-2779. https://doi.org/10.1021/cm050106z

[30] Ebbesen, S.D., Jensen, S.H., Hauch, A. and Mogensen, M.B. (2014) High Temperature Electrolysis in Alkaline Cells, Solid Proton Conducting Cells, and Solid Oxide Cells. *Chemistry of Materials*, **114**, 10697-10734. https://doi.org/10.1021/cr5000865

[31] Goodenough, J.B. and Zhou, J.-S. (1998) Localized to Itinerant Electronic Transitions in Transition-Metal Oxides with the Perovskite Structure. *Chemistry of Materials*, **10**, 2980-2993. https://doi.org/10.1021/cm980276u

[32] Whangbo, M.-H., Koo, H.-J., Villesuzanne, A. and Pouchard, M. (2002) Effect of Metal-Oxygen Covalent Bonding on the Competition between Jahn-Teller Distortion and Charge Disproportionation in the Perovskites of High-Spin d^4 Metal Ions $LaMnO_3$ and $CaFeO_3$. *Inorganic Chemistry*, **41**, 1920-1929. https://doi.org/10.1021/ic0110427

[33] Jiang, L., Saldana-Greco, D., Schick, J.T. and Rappe, A.M. (2014) Enhanced Charge Ordering Transition in Doped $CaFeO_3$ through Steric Templating. *Physical Review B*, **89**, Article ID: 235106. https://doi.org/10.1103/PhysRevB.89.235106

[34] Takashima, T., Hashimoto, K. and Nakamura, R. (2012) Mechanisms of pH-Dependent Activity for Water Oxidation to Molecular Oxygen by MnO_2 Electrocatalysts. *Journal of the American Chemical Society*, **134**, 1519-1527. https://doi.org/10.1021/ja206511w

[35] Takashima, T., Hashimoto, K. and Nakamura, R. (2012) Inhibition of Charge Disproportionation of MnO_2 Electrocatalysts for Efficient Water Oxidation under Neutral Conditions. *Journal of the American Chemical Society*, **134**, 18153-18156. https://doi.org/10.1021/ja306499n

[36] Takashima, T., Yamaguchi, A., Irie, H., Hashimoto, K. and Nakamura, R. (2014) *In Situ* UV-vis Absorption Spectra of Intermediate Species for Oxygen-Evolution Reaction on the Surface of MnO_2 in Neutral and Alkaline Media. *Electrochemistry*, **82**, 325-327. https://doi.org/10.5796/electrochemistry.82.325

[37] Axmann, P., Erdbrügger, C.F., Buss, D.H. and Glemser, O. (1996) Formation of Fe^{IV} and Ni^{IV} by Electrochemical and Chemical Oxidation of an Iron-Substituted Nickel (II) Hydroxide: The Direct Two-Electron Step $Ni^{II} \rightarrow Ni^{IV} + 2e^{-}$. *Angewandte Chemie International Edition*, **35**, 1115-1118. https://doi.org/10.1002/anie.199611151

[38] Hamen, H.C.B. and Koch, C.B. (1994) Iron (IV) in Layered Cobalt-Iron Oxide Formed by Electrochemical Oxidation. *Inorganic Chemistry*, **33**, 5363-5365. https://doi.org/10.1021/ic00101a034